Spin valve effect in VN/GaN/VN van der Waals heterostructures

Haoshen Ye,[1] Yijie Zhu,[1] Dongmei Bai,[2] Junting Zhang,[1] Xiaoshan Wu,[3] and Jianli Wang[1,*]
[1]*School of Materials and Physics, China University of Mining and Technology, Xuzhou 221116, China*
[2]*School of Mathematics, China University of Mining and Technology, Xuzhou 221116, China*
[3]*National Lab of Solid State Microstructures, Nanjing University, Nanjing 210093, China*

(Received 9 April 2020; revised 6 December 2020; accepted 7 January 2021; published 22 January 2021)

Nitride-based van der Waals magnetic heterostructures can simultaneously utilize both charge and spin degrees of electrons, which are important materials for low-dimensional spintronic devices. In this work, we study the stabilities and the electronic and magnetic properties of GaN/VN and VN/GaN/VN van der Waals heterostructures via first-principles calculations. The GaN/VN van der Waals heterostructure is a half-metal with 100% spin polarization, which can be applied in a spin filter and spin injection. Although monolayer GaN is a nonmagnetic semiconductor, it can introduce half-metallic characters via the magnetic proximity effect in both GaN/VN and VN/GaN/VN van der Waals heterostructures. The easy magnetization axis of hexagonal VN transits from the out-of-plane to the in-plane direction after combining with hexagonal GaN due to the different orbital occupations. Moreover, the electronic properties of the VN/GaN/VN van der Waals heterostructure depend largely on the magnetic configurations of the VN layers. By applying parallel or antiparallel magnetic configurations, the VN/GaN/VN van der Waals heterostructure presents half-metallic and semiconducting characters. The transformation indicates that the VN/GaN/VN van der Waals heterostructure is a promising candidate for room-temperature van der Waals spin valve devices.

DOI: 10.1103/PhysRevB.103.035423

I. INTRODUCTION

As is known, electrons have two basic degrees of freedom: electrical charge and spin. Mainstream electronics and devices are charge-based, while the electron spin is usually neglected [1,2]. Due to the current urgent demand for miniaturization, low power consumption, and high performance of electronic devices, low-dimensional spintronic materials have attracted much attention [3–5]. The response speed of charge-based electronics is limited by the current and capacitance of the devices. Comparatively, the response speed of spintronics depends on the frequency of electronic spin, which ranges from GHz to THz. Furthermore, reversing the spin direction only requires an meV of energy in spintronics [6]. Magnetism is a basic requirement of spin-based devices, which can be introduced by constructing the van der Waals (vdW) heterostructures with two-dimensional (2D) vdW magnetic crystals [5]. Bulk GaN is a semiconducting material that has advantages in technological applications, such as light-emitting diodes [7], lasers [8], and radiofrequency amplifiers [9]. Fortunately, 2D hexagonal GaN has been synthesized by migration-enhanced encapsulated growth [10]. The 2D GaN and GaN-based 2D vdW heterostructures are found to be alternative materials for deep ultraviolet light-emitting diodes [11,12], and some others show the potential for photocatalysis [13,14]. However, the intrinsic nonmagnetism of pristine 2D GaN limits its application in nanospintronic devices. Interestingly, under certain conditions, 2D GaN can be switched to a half-metal [15], which is a unique material that is able to achieve 100% spin-polarized current. In the band structure of a half-metal, the band gap exists in only one spin direction, while in the other spin direction it behaves like a metal [16]. Spin-polarized current is capable of using the electronic spin to deliver and store information. Therefore, half-metals can be an alternative candidate for spintronics and spin-based devices.

Half-metal can be easily found in ferromagnets because intensive magnetism results in different behaviors of electrons with different spin directions. So far, investigations of half-metallic ferromagnets have focused mainly on double perovskite materials [17], Heusler alloys [18], and transition-metal compounds [19,20]. In addition, the combination of 2D ferromagnets and 2D semiconductors is advantageous because proximity-induced exchange interaction can lead to entirely new spintronics and valleytronics [21,22]. Therefore, the vertical integration of ferromagnets and 2D monolayer GaN into vdW heterostructures with atomically sharp interfaces is an effective way to obtain magnetism via the magnetic proximity effect [23]. Meanwhile, experimentally high-quality vdW heterostructures can be precisely and controllably synthesized by creating a periodic array of defects on the substrate [24]. The 2D hexagonal VN is a ferromagnetic (FM) half-metal with an ultrahigh Curie temperature of 768 K [25]. Large spin and valley splitting can be found in WS_2/VN vdW heterostructures [26]. These results suggest that both monolayer VN and VN-based heterostructures can be used in spintronics, information memories, and storage devices. The spin valve is a typical spintronic with a sandwich structure in which the first and third layers are ferromagnets and the second layer is a nonmagnetic material. The

*Author to whom all correspondence should be addressed: jlwang@cumt.edu.cn

magnetoresistance of a spin valve is determined by the magnetization directions of the ferromagnets, which can be realized in the vdW spin valves as well [27,28]. The spin valves play an important role in magnetic field sensors [29], memory devices [30,31], and even biological fields [32]. In this work, we study the electronic properties of VN/GaN vdW heterostructures and VN/GaN/VN vdW spin valves via first-principles simulations. The VN/GaN/VN vdW spin valve is also a trilayer vdW heterostructure. Meanwhile, the correspondence of the heterostructures under strain is investigated.

II. METHODOLOGY

The optimal atomic structures and electronic properties of monolayer VN, monolayer GaN, and their heterostructures rely on first-principles calculations via the Vienna Ab-initio Simulation Package [33]. The cutoff energy for the plane-wave basis is set to 600 eV. To eliminate the interlayer interaction, a 20-Å-thick out-of-plane vacuum space is applied. Numerical integration over the Brillouin zone is sampled with the Monkhorst-Pack scheme with a $12 \times 12 \times 1$ k-point mesh [34]. The exchange-correlation potential is described with the Perdew-Burke-Ernzerhof generalized gradient approximation (GGA) [35]. The D3 Grimme correction is also adopted for the consideration of vdW interactions in all computational processes [36]. All the atomic coordinates, the lattice constants, and the depth of the interlayer are given by full relaxation with a maximum residual force of 0.01 V Å^{-1}. The maximum of the residual total energy is set to 10^{-6} eV. Spin-orbital coupling (SOC) is applied when searching for the easy magnetic axes [37,38]. The screened hybrid density functional proposed by Heyd, Scuseria, and Ernzerhof (HSE06) is used to solve the band structures [39]. For comparison, calculations based on the GGA+U method are also carried out. The effective Hubbard U correction applied on the 3d electrons of vanadium atoms is 3.47 eV (see the Supplemental Material [40] for details). The linear response theory is adopted to evaluate the U parameter [41], which is widely used in evaluating the U parameters of the transition atoms [42–44]. The phonon properties are carried out with $5 \times 5 \times 1$ supercells using the PHONOPY code. The Curie temperatures (T_c) of the magnetic systems are estimated via Monte Carlo (MC) simulations with $15 \times 15 \times 1$ supercells.

III. RESULTS AND DISCUSSION

As presented in Figs. 1(a) and 1(b), both isolated GaN and isolated VN have graphenelike crystal structures without corrugation. The optimal lattice constants of monolayer GaN and monolayer VN are $a_{\mathrm{GaN}} = b_{\mathrm{GaN}} = 3.20$ Å and $a_{\mathrm{VN}} = b_{\mathrm{VN}} = 3.23$ Å, respectively. The Ga-N and V-N bond lengths are 1.85 and 1.86 Å, respectively. The magnetic moment of the monolayer VN is 1.97 μ_{B} per unit cell, and the monolayer GaN is nonmagnetic. These results are in agreement with previous works [25,45]. The lattice mismatch of the monolayer GaN and the monolayer VN is 0.93%, which is acceptable to form a heterostructure. Initially, we consider six different high symmetric configurations for the GaN/VN vdW heterostructures. The binding energies of different configurations are compared by employing $E_b = E_{\mathrm{GaN/VN}} - E_{\mathrm{GaN}} - E_{\mathrm{VN}}$, in which

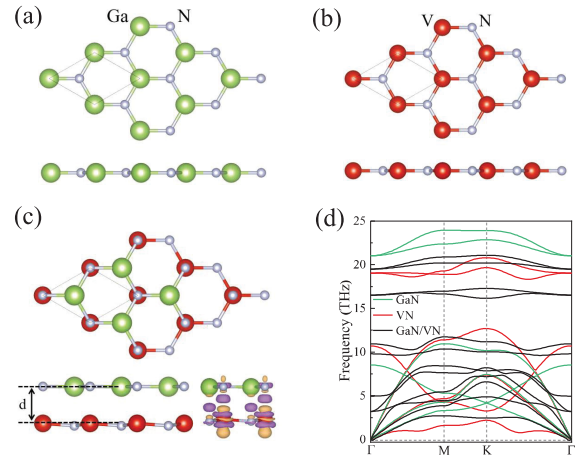

FIG. 1. The top view and side view of (a) monolayer GaN, (b) monolayer VN, and (c) GaN/VN vdW heterostructure; the purple and orange distributions correspond to charge accumulation and depletion with an isosurface value of 0.03 e Å^{-3}, respectively; (d) the phonon spectra of monolayer GaN, monolayer VN, and GaN/VN vdW heterostructure.

$E_{\mathrm{GaN/VN}}$, E_{GaN}, and E_{VN} are the total energy of the GaN/VN heterostructures, the monolayer GaN, and the monolayer VN, respectively. The most thermodynamically favorable configuration is presented in Fig. 1(c) with calculated $E_b = -0.7$ eV. The metallic atoms match the nonmetallic atoms of the other layer, and the VN layer exhibits corrugation, which is consistent with the WS_2/VN vdW heterostructure and the VN/MoS_2 heterostructure [25,26]. On the other hand, among the six high symmetric configurations, only the stacking configuration [as shown in Fig. 1(c)] has no obvious imaginary vibrational modes in phonon spectra. However, imaginary vibrational modes have been seen in the calculated results of the other stacking configurations (see Fig. S6 of the Supplemental Material [40]). Moreover, monolayer GaN, monolayer VN, and the GaN/VN vdW heterostructure remain stable under -1% to 5%, 0% to 5%, and -2% to 5% biaxial strains, respectively (see Fig. S8 of the Supplemental Material [40]). The magnetic ground states of both the monolayer VN and the GaN/VN vdW heterostructure are FM states, regardless of whether there is a Hubbard U correction or not. The lattice constants of the GaN/VN vdW heterostructure are $a_{\mathrm{GaN/VN}} = b_{\mathrm{GaN/VN}} = 3.28$ Å and the length of the V-N bond increases to 1.89 Å. The distance between the two layers is 2.22 Å and it is larger than that of the V-N bond, indicating that chemical bonds are absent between the layers. The magnetic moment of the VN layer decreases to 1.75 μ_{B} per unit cell and the GaN layer obtains a small amount of magnetic moment of 0.02 μ_{B}. As can be seen in Fig. 1(c), the charge mainly accumulates at the interface of the GaN/VN heterostructure, and charge transfer mainly happens on vanadium atoms. According to Bader charges analysis [46,47], the GaN layer obtains 0.0575 e from the VN layer. These results indicate that orbital hybridization exists in the GaN/VN vdW heterostructure.

The band structures of monolayer GaN and monolayer VN are presented in Fig. 2. The conduction-band minimum (CBM) and valence-band maximum (VBM) of monolayer GaN are located at the Γ point and the K point, showing

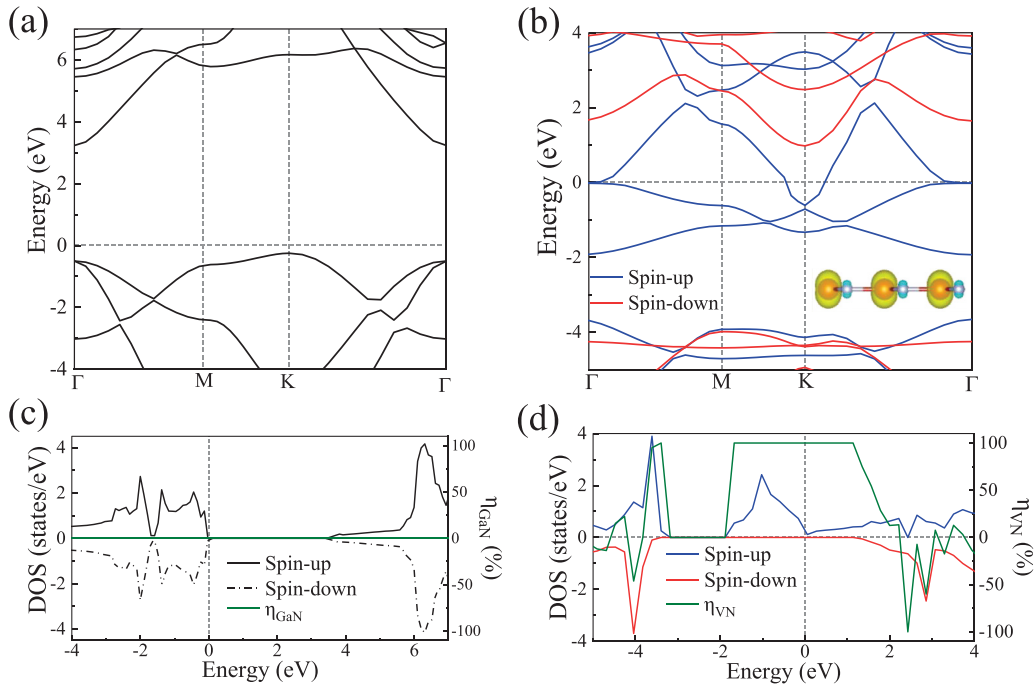

FIG. 2. Band structures of (a) monolayer GaN and (b) monolayer VN. The inset shows the spin-polarized charge distribution of monolayer VN. The yellow and blue distributions correspond to spin-up and spin-down polarized charge with an isosurface value of 0.2 e Å^{-3}. The DOS and spin polarization of (c) monolayer GaN and (d) monolayer VN.

the features of the indirect semiconductor. The value of the band gap is 3.48 eV, which is close to that of previous works [10,45]. Because monolayer GaN is a nonmagnetic material, the band structure of spin-up and spin-down channels is degenerate. That is, there is no spin polarization in monolayer GaN. We estimate the spin polarization level through the density of states (DOS) by using $\eta = 100\% \times (n_\uparrow - n_\downarrow)/(n_\uparrow + n_\downarrow)$, in which $n_\uparrow$ and $n_\downarrow$ are the DOS donated by spin-up and spin-down electrons, respectively. The positive and negative values of η correspond to spin-up and spin-down polarization, respectively. As shown in Fig. 2(c), the DOSs with different spin directions are completely symmetrical, resulting in $\eta_{GaN} = 0\%$ for the monolayer GaN. As for the monolayer VN, the spin-polarized charge distribution is presented in the inset of Fig. 2(b). The spin-up polarized charge is completely distributed on vanadium atoms, and the spin-down polarized charge is distributed only slightly on nitrogen atoms. The spin-up and spin-down band structures of monolayer VN are nondegenerate. The spin-up electrons cross the Fermi energy level, while an indirect band gap of 4.96 eV appears in spin-down channels, which is a typical band structure of half-metals. The DOS of monolayer VN is presented in Fig. 2(d), and there is a large energy range near the Fermi energy level that can be 100% spin-polarized, which is the main demand of spin injection to create spin-polarized current [1,16,48].

Note that vertical vdW heterostructures constructed by monolayer GaN and monolayer VN can also produce highly spin-polarized current. The band structure of the GaN/VN vdW heterostructure is presented in Fig. 3(a), where the spin-up channels are conductive and spin-down channels have an indirect band gap with a value of 4.12 eV. As the spin-polarized charge distribution is shown in the inset of Fig. 3(a), it is obvious that the spin-up polarized charge of vanadium atoms is different from that of monolayer VN. The different spin-polarized charge distributions suggest that different magnetic properties may exist between the GaN/VN vdW heterostructure and the monolayer VN. As is shown in the partial DOS (PDOS) [Fig. 3(b)], both GaN and VN layers in the GaN/VN vdW heterostructure can realize 100% spin polarization at the Fermi energy level. The DOSs of spin-up and spin-down channels are asymmetric in the GaN layer, which is quite different from the isolated GaN [see Fig. 3(b)]. The half-metallic properties of the GaN layer in the GaN/VN vdW heterostructure are attributed to the *s-d* hybridization [Fig. 3(c)], where the s and d orbitals are donated by the nitrogen atom of GaN and the vanadium atom of VN, respectively. However, *p-d* hybridization also happens in the lower region of the valence band, which is far from the Fermi energy level. The spin polarization of the GaN/VN vdW heterostructure is also $\eta_{GaN/VN} = 100\%$ at the Fermi energy level, and electrons are 100% spin-up polarized in a large energy range of -2.55 to 0 eV below the Fermi energy level. In addition, in the energy range of 1.49–1.92 eV above the Fermi energy level, a completely spin-down polarized range appears, which does not exist in monolayer VN. Carrier doping may be an effective method to achieve the transition between spin-up and spin-down polarization [49–51].

To find out the easy magnetization axes of monolayer VN and the GaN/VN vdW heterostructure, we carry out calculations on magnetic anisotropy energy (MAE), which is given by comparing the total energy with the magnetization axis in different directions. As presented in Fig. 4, the easy magnetization axes of monolayer VN and the GaN/VN vdW heterostructure are the out-of-plane and in-plane directions, respectively. Experimentally, external magnetic fields can be

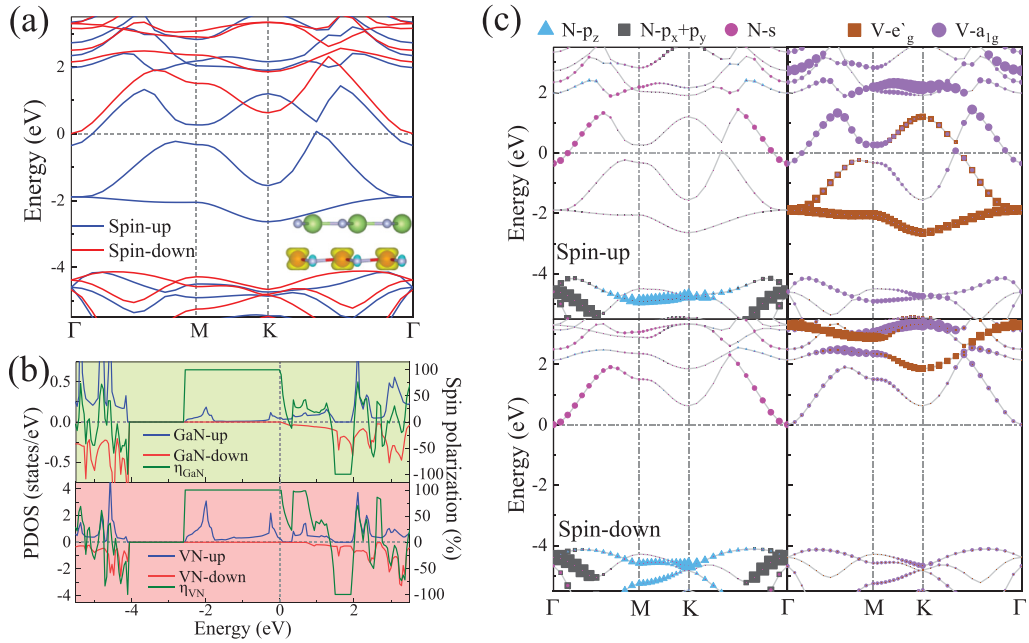

FIG. 3. (a) Band structure and spin-polarized charge distribution, (b) PDOS and spin polarization, and (c) orbital-projected band structure of the GaN/VN vdW heterostructure. The nitrogen atom and the vanadium atom are donated by GaN and VN, respectively. The yellow and blue distributions correspond to spin-up and spin-down polarized charge with an isosurface value of 0.2 e Å^{-3}, respectively.

perpendicularly or parallelly applied to the devices to tune the magnetization directions of materials [52,53]. It should be noted that both Hubbard U correction and biaxial strains cannot change the direction of the easy magnetization axes of these systems (Fig. 4 and Fig. S9 of the Supplemental Material [40]). The MAE of the monolayer VN and the GaN/VN vdW heterostructure are 0.14 and 0.26 meV at the GGA level, respectively. The Hubbard U correction reduces 0.1 meV on the MAE of monolayer VN while it increases 0.93 meV in the case of the GaN/VN vdW heterostructure (see Table S3 of the Supplemental Material [40]).

To explain the change of the easy magnetization axis of VN layers and the half-metallic property in the GaN layer, we investigated the crystal fields of the systems. According to the D_{3h} and C_{3v} point-group symmetry of the monolayer VN and the GaN/VN vdW heterostructure, the trigonal crystal field splits the d orbitals into three groups: e_g (d_{xy}, $d_{x^2-y^2}$), e'_g (d_{xz}, d_{yz}), and a_{1g} (d_{z^2}) [54], presented in Figs. 5(c) and 5(d). The orbital-projected DOS of the monolayer VN is presented in Fig. 5(a). The p_x and p_y orbitals of nitrogen atoms are hybridized with the e'_g orbital of vanadium atoms, forming the complanate σ bonds and resulting in the hexagonal atomic structure of 2D VN. The e_g orbital crosses the Fermi energy level, providing the half-metallic character of the monolayer VN. In the case of monolayer VN, the a_{1g} orbital is occupied and the e'_g orbital is half-filled. This orbital occupation of

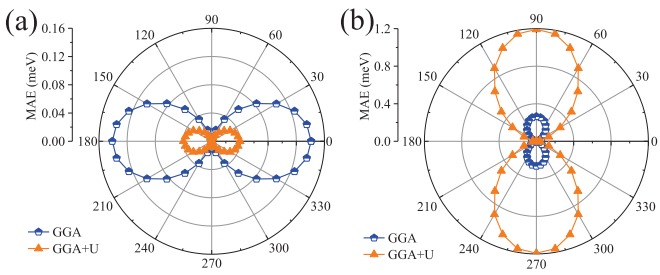

FIG. 4. The MAE of (a) monolayer VN and (b) GaN/VN vdW heterostructure at GGA and GGA+U level. 0° and 90° correspond to the in-plane and out-of-plane directions, respectively.

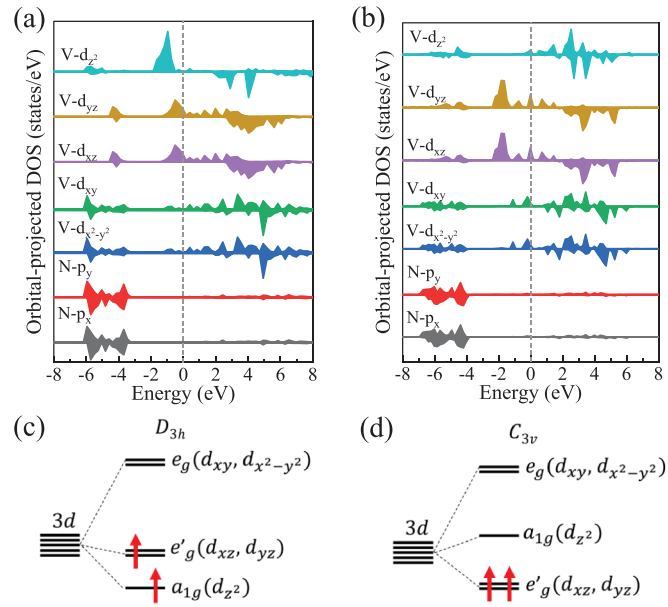

FIG. 5. Orbital-projected DOS of (a) monolayer VN and (b) VN layer of GaN/VN vdW heterostructure at HSE06 level. The trigonal crystal field level diagrams of vanadium atoms in (c) monolayer VN and (d) VN layer of GaN/VN vdW heterostructure.

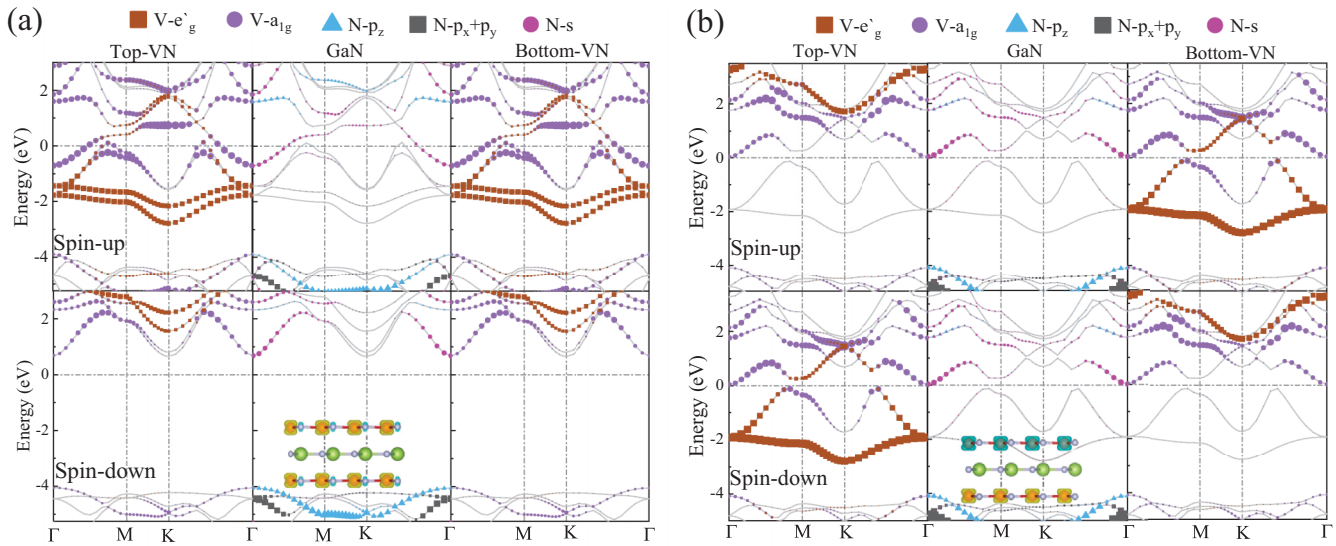

FIG. 6. The orbital-projected band structures of the VN/GaN/VN vdW heterostructure with (a) PM and (b) APM configurations, respectively. The nitrogen atom and the vanadium atom are donated by GaN and VN, respectively. The yellow and blue distributions correspond to spin-up and spin-down polarized charge with an isosurface value of 0.3 e Å^{-3}, respectively.

$a_{1g}{}^1 e'_g{}^1$ results in the out-of-plane easy magnetization axis [55]. Moreover, the magnetic anisotropy can be understood from second-order perturbation theory analysis [56]. The contribution to the SOC induced change in the MAE is given by

$$E^{\mathrm{SL}} = \sum_o \sum_u \frac{|\langle o|H^{\mathrm{SL}}|u\rangle|^2}{E_u - E_o},$$

where o and u correspond to the occupied and unoccupied states near the Fermi energy level, respectively; E_o and E_u are the energy levels of the states. $H^{\mathrm{SL}} = \xi \vec{\sigma} \cdot \vec{L}$, where ξ, $\vec{\sigma}$, and $\vec{L}$ are the SOC constant, the Pauli matrix, and an orbital angular momentum operator. Thus, when z and x denote the out-of-plane and in-plane directions, the MAE can be approximately estimated as

$$\Delta E = E(x) - E(z) = \pm\xi^2 \sum_{o,u} \frac{|\langle o|L_z|u\rangle|^2 - |\langle o|L_x|u\rangle|^2}{E_u - E_o},$$

where $\pm$ is decided by the spin states of the occupied and unoccupied states ($+$ and $-$ for parallel and opposite spin states, respectively). Four SOC interactions should be considered: $\Delta E^{\uparrow\uparrow}$, $\Delta E^{\downarrow\downarrow}$, $\Delta E^{\uparrow\downarrow}$, and $\Delta E^{\downarrow\uparrow}$. Negative and positive values of the total ΔE ($\Delta E_{\mathrm{total}}$) mean the in-plane and out-of-plane easy magnetization axis of the system. Based on detailed calculation (see the Supplemental Material [40] for details), the positive value of total $\Delta E_{\mathrm{total}}$ indicates the out-of-plane easy magnetization axis of monolayer VN. In the case of the GaN/VN vdW heterostructure [Fig. 5(b)], the orbital occupation configuration of the VN layer transits from $a_{1g}{}^1 e'_g{}^1$ to $e'_g{}^2$ [Fig. 5(d)] and the calculated $\Delta E_{\mathrm{total}}$ is negative. The transition of the orbital occupation results in the in-plane easy magnetization axis. The a_{1g} orbital is lifted over the Fermi energy level by the Coulomb repulsion from the charge accumulated at the interface of the GaN/VN vdW heterostructure [see Fig. 1(c)]. The spatial charge distribution of the a_{1g} orbital mainly extends along the out-of-plane direction (see Table S1 of the Supplemental Material [40]), which is inhibited by the interfacial charge. The Coulomb repulsion moves up the energy of the a_{1g} orbital, which results in electrons of the a_{1g} orbital transfering to the e'_g orbital. At the GGA+U level, all the peaks shift closer to the Fermi energy level (see Fig. S3 of the Supplemental Material [40]). Meanwhile, the orbital occupation configurations at the GGA+U level are the same as the results obtained from the HSE06 method.

Based on the stable GaN/VN vdW heterostructure, we construct a sandwich VN/GaN/VN vdW heterostructure by adding another VN layer on the GaN/VN vdW heterostructure. Compared to the bilayer vdW heterostructure, the different magnetic configurations of the VN layers in the trilayer vdW heterostructure can provide another effective method to tune the electronic properties. Different magnetic configurations are presented in the inserts of Figs. 6(a) and 6(b), corresponding to the parallel magnetic (PM) configuration and the antiparallel magnetic (APM) configuration, respectively. These magnetic configurations can be accomplished in experiments by applying external magnetic fields [52,53]. The magnetic ground state of the VN/GaN/VN vdW heterostructure is FM (see Fig. S5 of the Supplemental Material [40]), where the VN layers have corrugations, and the total magnetic moments are 3.60 μ_{B} and 0 μ_{B} per unit cell of the PM and APM configurations, respectively. The MAEs of the VN/GaN/VN vdW heterostructure are 0.10 and 0.39 meV at the GGA and GGA+U levels (see Table S3 of the Supplemental Material [40]), respectively. The crystal-field splitting in the VN/GaN/VN vdW heterostructure is the same as that in the VN/GaN vdW heterostructure [Fig. 5(d)]. Therefore, the easy magnetization axis of the VN/GaN/VN vdW heterostructure is also in the in-plane direction.

The orbital-projected band structure of the VN/GaN/VN vdW heterostructure with the PM configuration is presented in Fig. 6(a). The spin-up channels are conductive and spin-down channels have a band gap with a value of 4.73 eV, showing half-metallic characters. The PDOS of the PM configuration is

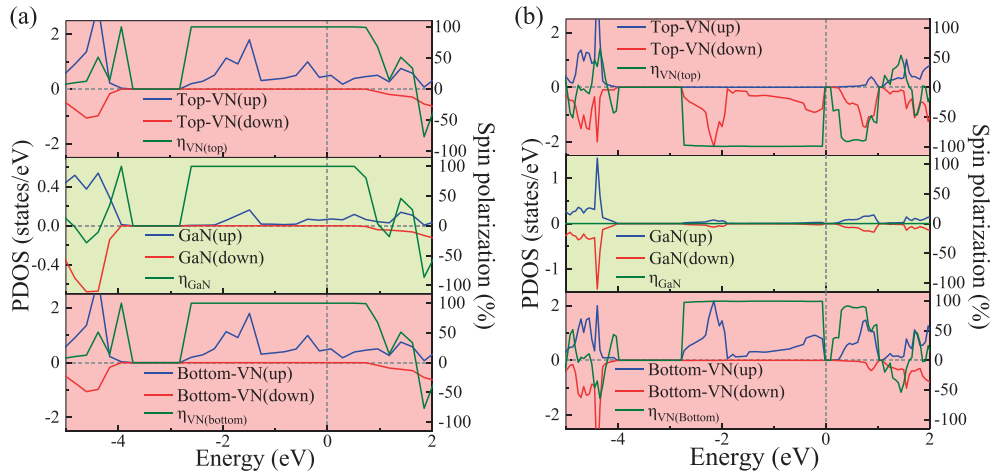

FIG. 7. PDOS and spin polarization of VN/GaN/VN vdW heterostructure with (a) PM and (b) APM configurations, respectively.

presented in Fig. 7(a) to study the spin polarization of different layers. In the energy range of −2.58 to 0.51 eV, electrons are 100% spin-up polarized, meaning that they can provide polarized in-plane current effectively. Though the VN layers provide the main spin-polarized channels at the Fermi energy level, spin-up channels of the GaN layer are also conductive. As with the GaN/VN vdW heterostructure, the half-metallic property of the GaN layer is attributed to the *s-d* hybridization [Fig. 6(a)]. Thus, the in-plane spin-polarized current can flow in every layer of the VN/GaN/VN vdW heterostructure. As for the APM configuration, the VN/GaN/VN vdW heterostructure presents semiconductor characters with a band gap of 0.16 eV in both spin channels [Fig. 6(b)]. The spin-up states of the top VN layer and the spin-down states of the bottom VN layer hybridize with the GaN layer in the same way and vice versa. That is, the same orbital hybridization happens in both the spin-up and spin-down channels in a similar way. Therefore, though *s-d* and *p-d* hybridization still exists in the VN/GaN/VN vdW heterostructure under an APM configuration, the GaN layer presents no spin polarization. In addition, a band gap exists in the energy range of 0.97–1.05 eV above the Fermi energy level, preventing electrons from entering higher energy levels. The band-gap value of 0.08 eV is much larger than that of 0.007 eV in the CrI_3/graphene/graphene/CrI_3 vdW spin valve [27]. As presented in Fig. 7(b), the top VN layer donates spin-down electrons while the bottom VN layer donates spin-up electrons near the Fermi energy level. The total spin polarization under an APM configuration is always below 0.78%, which is attributed to the highly symmetric total DOS. The gaps with the values of 0.16 and 0.08 eV in different energy ranges split electrons and holes effectively. From this standpoint, the in-plane conductance of the VN/GaN/VN vdW heterostructure with an APM configuration is supposed to be much lower than that of a PM configuration.

Due to the important role of T_c in the practical applications of spintronics, we adopted the MC simulation based on the Heisenberg model to estimate the T_c of magnetic systems (see the Supplemental Material [40] for details). The T_c of monolayer VN, the GaN/VN vdW heterostructure, and the VN/GaN/VN vdW heterostructure are above room temperature with values of 554.30, 443.04, and 531.65 K [Figs. 8(a) and 8(b)], respectively. Furthermore, the half-metallic property of the GaN/VN vdW heterostructure and the spin valve effect of the VN/GaN/VN vdW heterostructure stay well under −2% to 2% and −1% to 3% biaxial strains, respectively (see Fig. S8 of the Supplemental Material [40]). By applying different magnetic configurations, the transition between half-metal and semiconductor suggests that the VN/GaN/VN vdW heterostructures have a great potential for the vdW spin valve. The conductive and semiconductive states of the VN/GaN/VN vdW heterostructure correspond to low and high resistance states of the spin valve devices. According to previous experiments [53,57,58], the PM configuration shows a low resistance state and the APM configuration shows a high resistance state. Figures 8(c) and 8(d) present a PM and an APM configuration of the spin valves based on the VN/GaN/VN

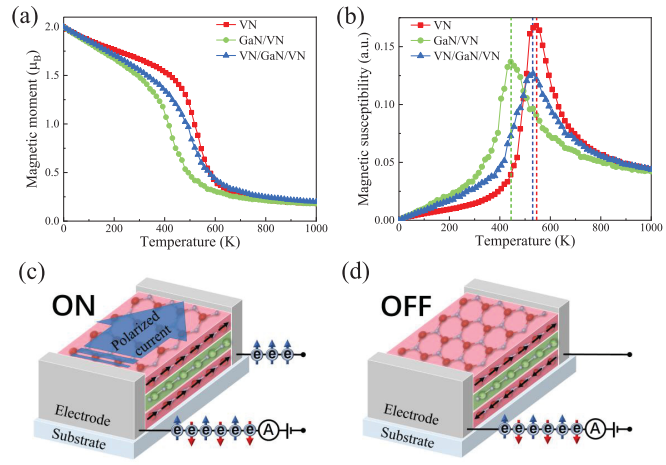

FIG. 8. The MC simulations of (a) magnetic moment and (b) magnetic susceptibility of monolayer VN, GaN/VN vdW heterostructure, and VN/GaN/VN vdW valve at the GGA level; the schematic diagrams for VN/GaN/VN vdW spin valves with (c) PM and (d) APM configurations. The black arrows correspond to magnetization directions of the FM VN layers; the blue and red arrows correspond to spin-up and spin-down electrons, respectively.

vdW heterostructure. In most cases of practical devices, the bottom FM layer is a pinned layer, whose magnetization direction cannot be changed by external magnetic fields. The other FM layer is a free layer, whose magnetization direction follows the external magnetic field. The resistance of the spin valve is able to switch abruptly between low and high states as the transition occurs between PM and APM configurations. Thus, the VN/GaN/VN vdW heterostructure can be applied in the spin valve transistors as magnetic field sensors by pinning the magnetization directions of the bottom VN layers [29]. If the direction of the magnetic field is parallel to the pinned layer, the vdW spin valve will display low in-plane resistance, and spin-polarized current can be detected. On the other hand, the different resistance states of the vdW spin valves are also necessary parts of magnetic random-access memory [30,31]. Applying magnetic fields to switch the resistance is the main method for writing information in spin valves.

IV. SUMMARY

We have systematically studied the magnetic and electronic properties of monolayer GaN, monolayer VN, and their vdW heterostructures. Structural and magnetic stabilities are studied via the phonon spectrum and the effect of Hubbard U correction. The GaN/VN vdW heterostructure is a ferromagnetic half-metal with 100% spin polarization, showing potential for application in spin filters and spin injection. Due to the *s-d* orbital hybridization, the GaN layer of the GaN/VN vdW heterostructure shows half-metal characters. The easy magnetization axes of the vdW heterostructures are different from that of monolayer VN, which is attributed to the different 3d orbital occupation configurations. The spin polarization of the GaN/VN vdW heterostructure is still higher than 90.8%, although it is transformed into metal under −5% through −3% compressive strains. Finally, under −1% through 3% strains, the VN/GaN/VN vdW heterostructure is capable of switching between a half-metal and a semiconductor by applying PM and APM configurations. All of these magnetic systems have a Curie temperature higher than room temperature. The transformation suggests that the VN/GaN/VN vdW heterostructure is a promising candidate for a room-temperature vdW spin valve.

ACKNOWLEDGMENTS

This work has been supported by the Fundamental Research Funds for the Central Universities under Grant No. 2020ZDPYMS28. We are grateful to the High-Performance Computing Center of China University of Mining and Technology for the award of CPU hours to accomplish this work.

[1] S. A. Wolf, D. D. Awschalom, R. A. Buhrman, J. M. Daughton, S. von Molnar, M. L. Roukes, A. Y. Chtchelkanova, and D. M. Treger, Science **294**, 1488 (2001).
[2] I. Zutic, J. Fabian, and S. D. Sarma, Rev. Mod. Phys. **76**, 323 (2004).
[3] S. Bhatti, R. Sbiaa, A. Hirohata, H. Ohno, S. Fukami, and S. N. Piramanayagam, Mater. Today **20**, 530 (2017).
[4] Y. P. Feng, L. Shen, M. Yang, A. Wang, M. Zeng, Q. Wu, S. Chintalapati, and C. R. Chang, WIREs Comput. Mol. Sci. **7**, e1313 (2017).
[5] W. Zhang, P. K. J. Wong, R. Zhu, and A. T. S. Wee, InfoMat. **1**, 479 (2019).
[6] D. D. Awschalom and M. E. Flatté, Nat. Phys. **3**, 153 (2007).
[7] H. S. Wasisto, J. D. Prades, J. Gülink, and A. Waag, Appl. Phys. Rev. **6**, 041315 (2019).
[8] K. H. Li, X. Liu, Q. Wang, S. Zhao, and Z. Mi, Nat. Nanotechnol. **10**, 140 (2015).
[9] H. Amano, Y. Baines, E. Beam, M. Borga, T. Bouchet, P. R. Chalker, M. Charles, K. J. Chen, N. Chowdhury, R. M. Chu, C. De Santi, M. M. De Souza, S. Decoutere, L. Di Cioccio, B. Eckardt, T. Egawa, P. Fay, J. J. Freedsman, L. Guido, O. Häberlen, G. Haynes, T. Heckel, D. Hemakumara, P. Houston, J. Hu, M. Y. Hua, Q. Y. Huang, A. Huang, S. Jiang, H. Kawai, D. Kinzer, M. Kuball, A. Kumar, K. B. Lee, X. Li, D. Marcon, M. März, R. McCarthy, G. Meneghesso, M. Meneghini, E. Morvan, A. Nakajima, E. M. S. Narayanan, S. Oliver, T. Palacios, D. Piedra, M. Plissonnier, R. Reddy, M. Sun, I. Thayne, A. Torres, N. Trivellin, V. Unni, M. J. Uren, M. Van Hove, D. J. Wallis, J. Wang, J. Xie, S. Yagi, S. Yang, C. Youtsey, R. Yu, E. Zanoni, S. Zeltner, and Y. H. Zhang, J. Phys. D **51**, 163001 (2018).
[10] Z. Y. Al Balushi, K. Wang, R. K. Ghosh, R. A. Vila, S. M. Eichfeld, J. D. Caldwell, X. Qin, Y. C. Lin, P. A. DeSario, G. Stone, S. Subramanian, D. F. Paul, R. M. Wallace, S. Datta, J. M. Redwing, and J. A. Robinson, Nat. Mater. **15**, 1166 (2016).
[11] A. Aiello, Y. Wu, A. Pandey, P. Wang, W. Lee, D. Bayerl, N. Sanders, Z. Deng, J. Gim, K. Sun, R. Hovden, E. Kioupakis, Z. Mi, and P. Bhattacharya, Nano Lett. **19**, 7852 (2019).
[12] Y. Wu, X. Liu, P. Wang, D. A. Laleyan, K. Sun, Y. Sun, C. Ahn, M. Kira, E. Kioupakis, and Z. Mi, Appl. Phys. Lett. **116**, 013101 (2020).
[13] M. A. Hassan, M. W. Kim, M. A. Johar, A. Waseem, M. K. Kwon, and S. W. Ryu, Sci. Rep. **9**, 20141 (2019).
[14] J. Li, W. J. Yang, A. M. Wu, X. L. Zhang, T. T. Xu, and B. D. Liu, ACS Appl. Mater. Interfaces **12**, 8583 (2020).
[15] H. M. Li, J. Dai, J. Li, S. Zhang, J. Zhou, L. J. Zhang, W. S. Chu, D. Chen, L. F. Zhao, H. J. L. Yang, and Z. Y. Wu, J. Phys. Chem. C **114**, 11390 (2010).
[16] J. H. Park, E. Vescovo, H. J. Kim, C. Kown, R. Ranesh, and T. Venkaresan, Nature (London) **392**, 794 (1998).
[17] K. I. Kobayashi, T. Kimura, H. Sawada, K. Terakura, and Y. Tokura, Nature (London) **395**, 677 (1998).
[18] P. J. Brown, K. U. Neumann, and P. J. Webster, and K. R. A. Ziebeck, J. Phys.: Condens. Matter **12**, 1827 (2000).
[19] Y. Qu, H. Pan, and C. T. Kwok, Sci. Rep. **6**, 34186 (2016).
[20] H. van Gog, W. F. Li, C. Fang, R. S. Koster, M. Dijkstra, and M. van Huis, npj 2D Mater. Appl. **3**, 18 (2019).
[21] D. Zhong, K. L. Seyler, X. Y. Linpeng, R. Cheng, N. Sivadas, B. Huang, E. Schmidgall, T. Taniguchi, K. Watanabe, M. A. McGuire, W. Yao, D. Xiao, K. M. C. Fu, and X. D. Xu, Sci. Adv. **3**, e1603113 (2017).
[22] X. Q. Wu, H. Meng, F. J. Kong, H. Y. Zhang, Y. J. Bai, and N. Xu, Phys. Rev. B **101**, 125406 (2020).

[23] D. Zhong, K. L. Seyler, X. Linpeng, N. P. Wilson, T. Taniguchi, K. Watanabe, M. A. McGuire, K. M. C. Fu, D. Xiao, W. Yao, and X. Xu, Nat. Nanotechnol. **15**, 187 (2020).
[24] J. Li, X. D. Yang, Y. Liu, B. L. Huang, R. X. Wu, Z. Zhang, B. Zhao, H. F. Ma, W. Q. Dang, Z. Wei, K. Wang, Z. Y. Lin, X. Yan, M. Z. Sun, B. Li, X. Q. Pan, J. Luo, G. Y. Zhang, Y. Liu, Y. Huang, X. D. Duan, and X. F. Duan, Nature (London) **579**, 368 (2020).
[25] A. V. Kuklin, S. A. Shostak, and A. A. Kuzubov, J. Phys. Chem. Lett. **9**, 1422 (2018).
[26] C. M. Ke, Y. P. Wu, W. H. Yang, Z. M. Wu, C. M. Zhang, X. Li, and J. Y. Kang, Phys. Rev. B **100**, 195435 (2019).
[27] C. Cardoso, D. Soriano, N. A. Garcia-Martinez, and J. Fernandez-Rossier, Phys. Rev. Lett. **121**, 067701 (2018).
[28] M. Modarresi, A. Mogulkoc, Y. Mogulkoc, and A. N. Rudenko, Phys. Rev. Appl. **11**, 064015 (2019).
[29] D. J. Monsma, J. C. Lodder, T. J. A. Popma, and B. Dieny, Phys. Rev. Lett. **74**, 5260 (1995).
[30] F. Bello, S. Sanvito, O. Hess, and J. F. Donegan, ACS Photon. **6**, 1524 (2019).
[31] I. A. Iusipova, Semiconductors **53**, 2029 (2020).
[32] W. L. Qiu, L. Chang, Y. C. Liang, J. Litvinov, J. Guo, Y. T. Chen, B. Vu, K. Kourentzi, S. Xu, T. R. Lee, Y. Zu, R. C. Willson, and D. Litvinov, Sens. Act. A **265**, 174 (2017).
[33] G. Kresse and J. Furthmüller, Phys. Rev. B **54**, 11169 (1996).
[34] H. J. Monkhorst and J. D. Pack, Phys. Rev. B **13**, 5188 (1976).
[35] J. P. Perdew, K. Burke, and M. Ernzerhof, Phys. Rev. Lett. **77**, 3865 (1996).
[36] S. Grimme, J. Antony, S. Ehrlich, and H. Krieg, J. Chem. Phys. **132**, 154104 (2010).
[37] X. D. Wang, D. S. Wang, R. Q. Wu, and A. J. Freeman, J. Magn. Magn. Mater. **159**, 337 (1996).
[38] G. H. O. Daalderop, P. J. Kelly, and M. F. H. Schuurmans, Phys. Rev. B **41**, 11919 (1990).
[39] J. Heyd, G. E. Scuseria, and M. Ernzerhof, J. Chem. Phys. **118**, 8207 (2003).
[40] See Supplemental Material at http://link.aps.org/supplemental/10.1103/PhysRevB.103.035423 for (i) Hubbard U corrections, (ii) structural and strains properties, (iii) details for second-order perturbation theory analysis, and (iv) Curie temperature.
[41] M. Cococcioni and S. de Gironcoli, Phys. Rev. B **71**, 035105 (2005).
[42] H. M. Le, T. T. Pham, T. S. Dinh, Y. Kawazoe, and D. Nguyen-Manh, J. Phys.: Condens. Matter **28**, 135301 (2016).
[43] E. B. Linscott, D. J. Cole, M. C. Payne, and D. D. O'Regan, Phys. Rev. B **98**, 235157 (2018).
[44] J. J. He, S. Y. Ma, P. B. Lyu, and P. Nachtigall, J. Mater. Chem. C **4**, 2518 (2016).
[45] A. Onen, D. Kecik, E. Durgun, and S. Ciraci, Phys. Rev. B **93**, 085431 (2016).
[46] R. F. W. Bader, Chem. Rev. **91**, 893 (1991).
[47] E. Sanville, S. D. Kenny, R. Smith, and G. Henkelman, J. Comput. Chem. **28**, 899 (2007).
[48] C. Felser, G. H. Fecher, and B. Balke, Angew. Chem. Int. Ed. **46**, 668 (2007).
[49] Y. J. Sun, Z. W. Zhuo, and X. J. Wu, J. Mater. Chem. C **6**, 11401 (2018).
[50] B. Wang, Q. S. Wu, Y. H. Zhang, Y. L. Guo, X. W. Zhang, Q. H. Zhou, S. Dong, and J. L. Wang, Nanoscale Horiz. **3**, 551 (2018).
[51] L. Liu, S. Liu, Z. Zhang, and W. Zhu, J. Phys. Chem. C **121**, 24824 (2017).
[52] Y. K. Luo, J. Xu, T. Zhu, G. Wu, E. J. McCormick, W. Zhan, M. R. Neupane, and R. K. Kawakami, Nano Lett. **17**, 3877 (2017).
[53] Z. Wang, D. Sapkota, T. Taniguchi, K. Watanabe, D. Mandrus, and A. F. Morpurgo, Nano Lett. **18**, 4303 (2018).
[54] G. B. Liu, W. Y. Shan, Y. G. Yao, W. Yao, and D. Xiao, Phys. Rev. B **88**, 085433 (2013).
[55] K. Yang, F. R. Fan, H. B. Wang, D. I. Khomskii, and H. Wu, Phys. Rev. B **101**, 100402(R) (2020).
[56] D. S. Wang, R. Q. Wu, and A. J. Freeman, Phys. Rev. B **47**, 14932 (1993).
[57] M. Z. Iqbal, G. Hussain, S. Siddique, and M. W. Iqbal, J. Magn. Magn. Mater. **441**, 39 (2017).
[58] M. Z. Iqbal, G. Hussain, S. Siddique, and M. W. Iqbal, J. Magn. Magn. Mater. **429**, 330 (2017).